# Supporting Information

## Globally Suppressed Dynamics in Ion-doped Polymers

Michael A. Webb, Umi Yamamoto, Brett M. Savoie, Zhen-Gang Wang, and Thomas F. Miller III*

*Division of Chemistry and Chemical Engineering, California Institute of Technology, Pasadena, California 91125, USA*

E-mail: tfm@caltech.edu

# Contents



# 1 Simulation Details

All simulations were performed using the LAMMPS simulation package[1] with GPU acceleration,[2,3] a velocity Verlet integrator with a 1 fs timestep, and a Nose-Hoover thermostat

and barostat to control the temperature and pressure. The employed force field for PEO[4,5] and $Li^+$[6] is the same as that described in previous studies[6–9] with additional parameters for $PF_6^-$ taken from a validated force field for ionic liquids.[10,11] Here, the use of $PF_6^-$ as the anion and a fixed-charge force field is motivated by simplicity rather than practicality, since we are generically interested in the behavior of a polymer electrolyte with a dissociating salt. Here, the $LiPF_6$ is almost entirely disassociated with the employed force field, and there are no salt-rich/pure-polymer domains that may lead to dynamic heterogeneities.[12,13] Future quantitative work may utilize polarizable force fields or more commercially relevant anions, like $TFSI^-$.

System preparation begins with constructing sixteen independent copies of a simulation cell, each consisting of a single PEO chain of 640 monomers ($M_n \approx$ 28,000 g/mol) with an initial conformation generated according to the RIS approximation.[14] The use of a long chain suppresses global chain diffusivity, which is not expected to contribute significantly to $Li^+$ diffusion for polymer electrolyte applications. Following minimization and condensation using a previous protocol,[8] the sixteen simulation cells are replicated for each concentration (to make a total of $5 \times 16 = 80$ simulation cells). Except for sixteen cells used to study the neat polymer, $Li^+$ and $PF_6^-$ are randomly inserted into the remaining simulation cells to obtain sixteen replicas at each $Li^+$ to oxygen ratio; in the case of the "dilute" simulations, a single $Li^+$ is inserted into the simulation cell, and the system is neutralized with a uniform background charge.[15] Each of the simulation cells are annealed for 25 ns at 500 K and equilibrated for 25 ns at 400 K before production runs of 100 ns at 400 K.

# 2 Ion-polymer Dynamics During Constant Coordination

The results from Fig. 1 of the main text are obtained directly from unbiased molecular dynamics (MD) simulations. Consequently, even at timescales less than the characteristic

hopping time (Fig. 1c of main text), the $Li^+$ mean-squared displacement (MSD) contains small contributions from $Li^+$ hopping that could affect the observed power-law scaling. Moreover, the data also is obtained from a mixture of $Li^+$ coordination structures, namely whether the $Li^+$ is complexed by one or two contiguous polymer chain segments, and the impact of coordination structure on $Li^+$ MSD and associated power-law scaling has not been previously studied. To explicitly investigate the ion-polymer dynamics without conflation from ion-hopping or different coordination structures, we enforce either intra-chain or inter-chain coordination of the $Li^+$ (Fig. S1a ); both coordination types are observed in unbiased MD simulations. The coordination structures are achieved with the use of weak harmonic restraints on the distance between oxygen atoms at the center of the polymer chain with a specific $Li^+$; all other atoms in the system are left unconstrained. Fig. S1b characterizes the ion-polymer co-diffusion for both types of coordination. A clear trend is that inter-chain coordination results in slower diffusion across all concentration regimes. This may have general implications for ion transport, since coordination by separate units is less favorable from the standpoint of rafting contributions to the $Li^+$ diffusivity. On the other hand, the differences between intra- and inter-chain coordination become less pronounced at higher concentrations, suggesting that other factors govern the ion-polymer co-diffusion. The power-law scalings (Fig. S1c) are qualitatively similar to those observed in Fig. 1b of the main text, confirming key observations. Namely, the power-law scaling for the $Li^+$ MSD in the dilute regime is greater than the expected $t^{0.6}$ Rouse-like behavior, and a Rouse-like scaling is approached as the salt concentration increases, albeit at later times compared to the neat polymer. These results combine to show that the major trends identified with respect to the $Li^+$ MSD and its power-law scaling are signatures of coupled ion-polymer motion.

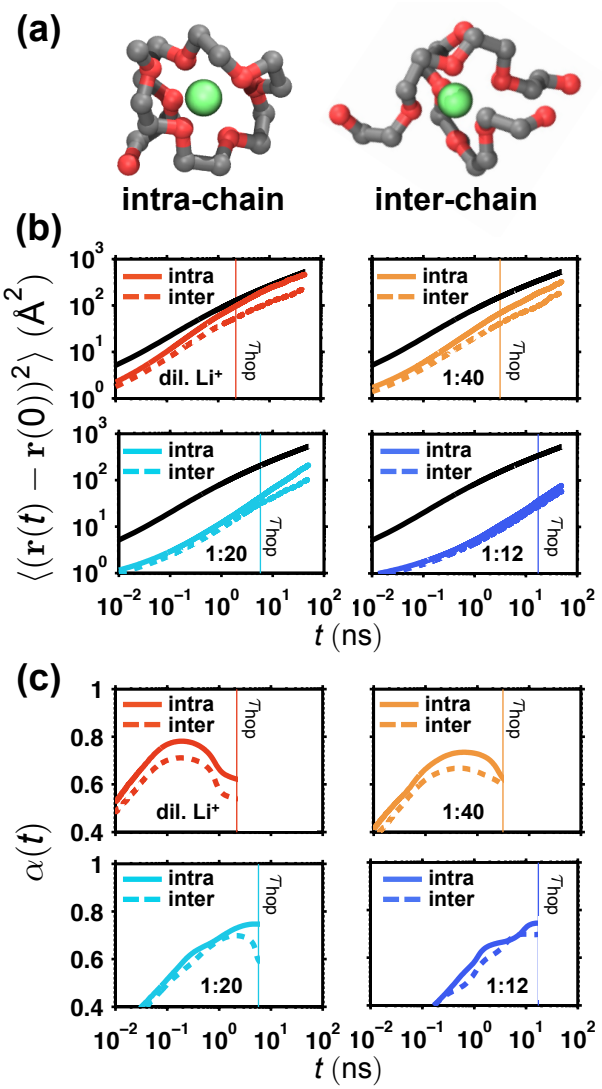


**Figure S1:** Comparison between inter-chain and intra-chain coordination motifs for $Li^+$-polymer co-diffusion. (a) Sample coordination motifs depicting intra-chain coordination and inter-chain coordination of $Li^+$ obtained from MD simulations. (b) Mean-squared displacement and (c) the corresponding time-dependent power-law scaling of the MSD for $Li^+$ for intra-chain and inter-chain coordination motifs at various salt concentrations up to the hopping time. In (b), the black lines indicate the mean-squared displacement of oxygen atoms in the neat polymer and are provided for reference. Similarly, the thin vertical lines indicate the $\tau_{\text{hop}}$ obtained from Fig. 1. The results in (b) and (c) are obtained for simulations that enforce a constant coordination condition.

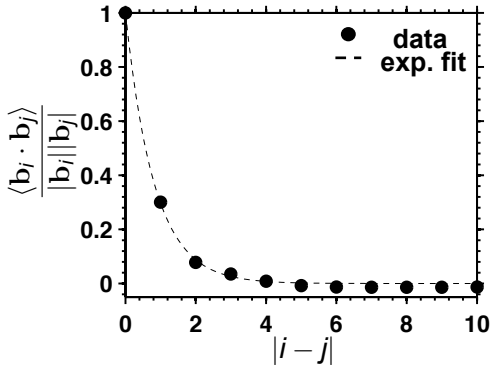


**Figure S2:** Evaluation of Gaussian/random-walk statistics for sub-chains of the neat polymer melt. Bond-vector correlation function used to identify the Kuhn length for PEO from the molecular dynamics simulations.

# 3 Rouse-mode Analysis Details

The Rouse-mode relaxation times presented in the main text are computed in three steps. First, we identify the Kuhn length for the polymer. Fig. S2 shows the bond vector correlation between monomers at increasing separations $|i-j|$, where $i$ and $j$ denote monomer indices. Although correlation-hole effects often cause deviations in chain structure for real chains,[16] PEO behaves as a Gaussian coil in its own melt,[17] and the data in Fig. S2 is adequately fit by an exponential function to yield a Kuhn length of approximately two monomers, which is consistent with previous studies.[17,18] Second, we perform a normal-mode analysis for a discrete polymer chain with $N = 320$ using

$$\mathbf{X}_p(t) = \frac{1}{N}\sum_{i=1}^{N} \mathbf{R}_i(t) \cos\left[\frac{p\pi}{N}\left(i - \frac{1}{2}\right)\right], \tag{S1}$$

where $\mathbf{X}_p(t)$ denotes the $p$th Rouse mode of the chain and $\mathbf{R}_i(t)$ is the Cartesian position of the $i$th bead of the polymer chain computed as the center-of-mass of the atoms comprising beads with indices $(2i-1)$ and $2i$. Third, relaxation times for each mode $\tau_p'$ are obtained as

$$\tau_p' = \frac{\tau_p}{\beta}\Gamma(\beta^{-1}), \tag{S2}$$

where the terms on the right-hand-side are determined by fitting the decay of $\mathbf{X}_p(t)$ to a Kohlrausch-William-Watts function, i.e., $\langle \mathbf{X}_p^2(t) \rangle \exp\left[-(t/\tau_p)^\beta\right]$. Fitting to the Kohlrausch-William-Watts function generally yields better results than a pure exponential function due to non-idealities that are present in realistically modeled systems.[19–23] For reference, the stretching coefficients computed from the fitting are providing in Fig. S3. The figure shows weak dependencies of the stretching coefficient $\beta$ on the mode number and the salt concentration. This indicates that the Rouse modes are not likely orthogonal in the atomistic system and exhibit coupling, and more complicated models may provide an overall better description. Nevertheless, combining the Rouse model with Eq. (S2) provides a reasonable way to compute length-scale dependent relaxation times, which is the primary interest in this work.

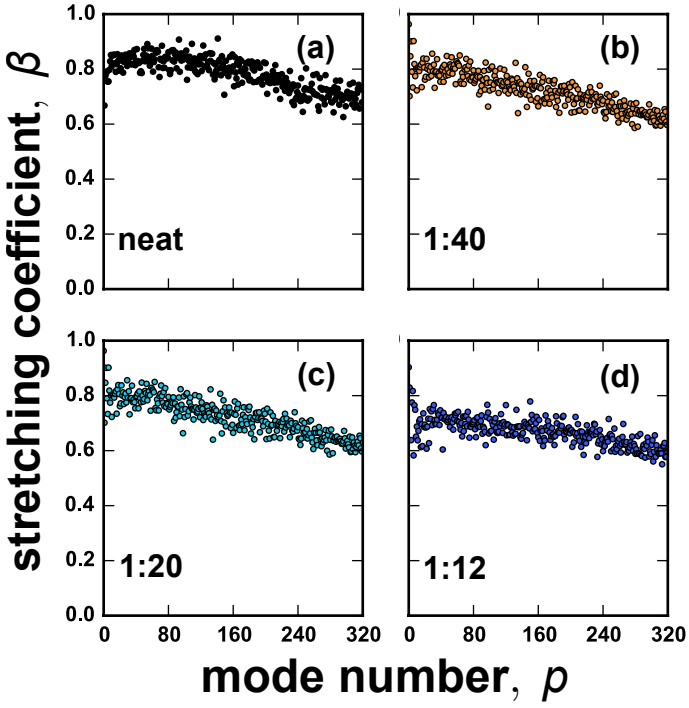


**Figure S3:** Stretching coefficients obtained from fitting the Kohlrausch-William-Watts function for relaxation of computed Rouse modes for (a) the neat polymer and polymer electrolytes with $Li^+$:O ratios of (b) 1:40, (c) 1:12, and (d) 1:20.

# 4 Internal Mean-squared Distance Between Monomers

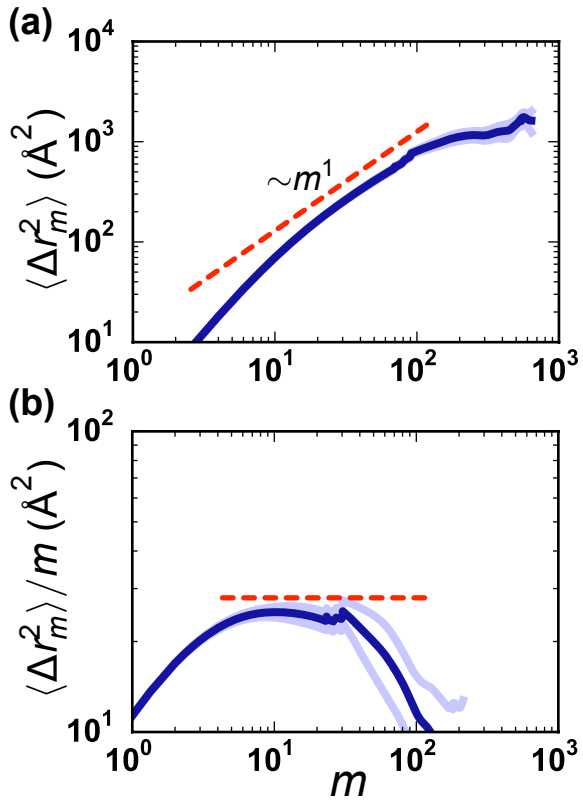


**Figure S4:** Evaluation of Gaussian/random-walk statistics for sub-chains of the neat polymer melt. (a) The mean-square end-to-end distance for sub-chains of $m$ monomers, $\langle \Delta r_m^2 \rangle$. (b) The mean-square end-to-end distance for sub-chains normalized by sub-chain size. In (a) and (b), the dashed red line illustrates the expected scaling for a random walk or a Gaussian chain, and the lighter blue lines indicate the standard error of the mean across the sixteen independent simulation cells.

Constructing the polymer melt using a single, long polymer chain simultaneously mitigates artifacts associated with ions interacting with the ends of polymer chains and limits the contribution of polymer center-of-mass diffusion to the $Li^+$ diffusivity. Because full equilibration of such a long polymer chain is not feasible in reasonable simulation time, we aim to restrict the Rouse relaxation-time analysis for the MD simulations (Fig. 2 of the main text) to length scales that are well equilibrated and obey Gaussian statistics. For a Gaussian chain, which is the basis of the Rouse model, the mean-square distance between monomers separated by $m-1$ monomers, or equivalently the end-to-end distance for a sub-chain of $m$

monomers, $\langle \Delta r_m^2 \rangle$, is expected to be a random walk that scales with $m$. Thus, to identify the largest sub-chain pertinent to our analysis, we utilize data from the inner two-thirds of the polymer chain (to avoid artifacts at the chain ends) to compute $\langle \Delta r_m^2 \rangle$ for all sub-chains of $m$ monomers. The results of these calculations are provided in Fig. S3a, which directly provides $\langle \Delta r_m^2 \rangle$, and S3b, which shows $\langle \Delta r_m^2 \rangle$ normalized by the sub-chain length. The power-law scaling in Fig. S3a and the plateau region in Fig. S3b indicate that Gaussian statistics are observed for sub-chains consisting of greater than about two monomers (determined as the Kuhn length in Fig. 2a of the main text) and fewer than about 30 monomers. Thus, the Rouse relaxation-time analysis is most reliable and relevant for the modes $1 \leq p \lesssim 22$. The apparent increased scatter in the data for $p < 22$ in Fig. 2b of the main text is likely an indicator that the polymer is not as well equilibrated at these larger length scales.

# 5 Comparison to Experiment

Recent work (published during the review of this manuscript) by Mongcopa et al.[24] used quasi-elastic neutron scattering to obtain monomeric friction coefficients as a function of salt concentration in PEO:LiTFSI polymer electrolytes; they showed the data was well fit by an exponential function. These measurements are relevant to Eq. 4 of the main text, which reports the monomeric friction employed in each bead as a function of salt mole fraction. Figure S5 shows the comparison between the experimental data obtained by Mongcopa et al.[24] (Ref. 39 of the main text) and a fit employing the functional form of Eq. 4 of the main text, namely $\frac{\zeta(x_s)}{\zeta_0} = 1 + ax_s + bx_s^2$ for $a \approx 1.8$ and $b \approx 2210$. The coefficients obtained here are similar in magnitude as the approximate coefficients employed in the main text, particularly when considering our coefficients are semiquantatively matched to simulation data of PEO:$LiPF_6$ at 400 K while these coefficients correspond to a system of PEO:LITFSI at 363 K. It is important to note that the simulated system corresponds to PEO:$LiPF_6$ at $T = 400$ K and the experimental system corresponds to PEO:LiTFSI at $T = 363$ K. Overall,

the fit describes the data very well and seemingly validates the use of Eq. 4 of the main text to describe the global changes in monomeric friction coefficient.

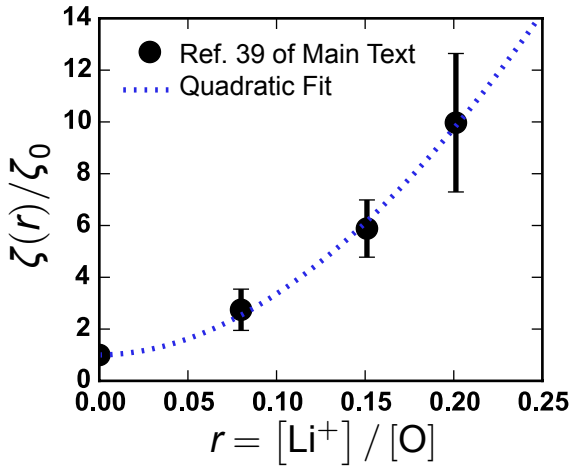


**Figure S5:** Comparison of experimental data for the normalized monomeric friction coefficient to a quadratic fit $\frac{\zeta(x_s)}{\zeta_0} = 1 + ax_s + bx_s^2$, akin to Eq. 4 of the main text. The experimental data from Mongcopa et al.[24] is obtained from quasi-elastic neutron scattering of PEO:LiTFSI polymer electrolytes at $T = 363K$. The fit employs $a \approx 1.8$ and $b \approx 2210$. Note that the data is fit using $x_s = \frac{r}{3+r}$ while the results are reported as a function $r$ to match the experimental presentation.

# References


(1) Plimpton, S. Fast Parallel Algorithms for Short-Range Molecular Dynamics. *J. Comp. Phys.* **1995**, *117*, 1 – 19.

(2) Brown, W. M.; Wang, P.; Plimpton, S. J.; Tharrington, A. N. Implementing Molecular Dynamics on Hybrid High Performance Computers - Short Range Forces. *Comput. Phys. Commun.* **2011**, *182*, 898–911.

(3) Brown, W. M.; Kohlmeyer, A.; Plimpton, S. J.; Tharrington, A. N. Implementing Molecular Dynamics on Hybrid High Performance Computers - Particle-Particle Particle-Mesh. *Comput. Phys. Commun.* **2012**, *183*, 449–459.

(4) Vanommeslaeghe, K.; Hatcher, E.; Acharya, C.; Kundu, S.; Zhong, S.; Shim, J.; Darian, E.; Guvench, O.; Lopes, P.; Vorobyov, I.; Mackerell, A. D. CHARMM general force field: A force field for drug-like molecules compatible with the CHARMM all-atom additive biological force fields. *J. Comput. Chem.* **2010**, *31*, 671–690.

(5) Stubbs, J. M.; Potoff, J. J.; Siepmann, J. I. Transferable Potentials for Phase Equilibria. 6. United-Atom Description for Ethers, Glycols, Ketones, and Aldehydes. *J. Phys. Chem. B* **2004**, *108*, 17596–17605.

(6) Wu, H.; Wick, C. D. Computational Investigation on the Role of Plasticizers on Ion Conductivity in Poly(ethylene oxide) LiTFSI Electrolytes. *Macromolecules* **2010**, *43*, 3502–3510.

(7) Webb, M. A.; Jung, Y.; Pesko, D. M.; Savoie, B. M.; Yamamoto, U.; Coates, G. W.; Balsara, N. P.; Wang, Z.-G.; Miller III, T. F. Systematic Computational and Experimental Investigation of Lithium-ion Transport Mechanisms in Polyester-based Polymer Electrolytes. *ACS Cent. Sci.* **2015**, 198–205.

(8) Webb, M. A.; Savoie, B. M.; Wang, Z.-G.; Miller III, T. F. Chemically Specific Dynamic Bond Percolation Model for Ion Transport in Polymer Electrolytes. *Macromolecules* **2015**, *48*, 7346–7358.

(9) Pesko, D. M.; Webb, M. A.; Jung, Y.; Zheng, Q.; Miller, T. F.; Coates, G. W.; Balsara, N. P. Universal Relationship between Conductivity and Solvation-Site Connectivity in Ether-Based Polymer Electrolytes. *Macromolecules* **2016**, *49*, 5244–5255.

(10) Canongia Lopes, J. N.; Deschamps, J.; Pádua, A. A. H. Modeling Ionic Liquids Using a Systematic All-Atom Force Field. *J. Chem. Phys. B* **2004**, *108*, 2038–2047.

(11) Canongia Lopes, J. N.; Pádua, A. A. H. Molecular Force Field for Ionic Liquids Composed of Triflate or Bistriflylimide Anions. *J. Chem. Phys. B* **2004**, *108*, 16893–16898.

(12) Borodin, O.; Smith, G. D. Molecular Dynamics Simulations of Poly(ethylene oxide)/LiI Melts. 1. Structural and Conformational Properties. *Macromolecules* **1998**, *31*, 8396–8406.

(13) Triolo, A.; Arrighi, V.; Triolo, R.; Passerini, S.; Mastragostino, M.; Lechner, R.; Ferguson, R.; Borodin, O.; Smith, G. Dynamic heterogeneity in polymer electrolytes. Comparison between QENS data and MD simulations. *Physica B: Condensed Matter* **2001**, *301*, 163 – 167.

(14) Flory, P. *Statistical mechanics of chain molecules*; Interscience Publishers, 1969.

(15) Figueirido, F.; Del Buono, G. S.; Levy, R. M. On finite-size effects in computer simulations using the Ewald potential. *The Journal of chemical physics* **1995**, *103*, 6133.

(16) Wang, Z.-G. 50th Anniversary Perspective: Polymer Conformation—A Pedagogical Review. *Macromolecules* **2017**, *50*, 9073–9114.

(17) Papadopoulos, G. D.; Tsalikis, D. G.; Mavrantzas, V. G. Microscopic Dynamics and Topology of Polymer Rings Immersed in a Host Matrix of Longer Linear Polymers:

Results from a Detailed Molecular Dynamics Simulation Study and Comparison with Experimental Data. *Polymers* **2016**, *8*.

(18) Mark, J. E.; Flory, P. J. The Configuration of the Polyoxyethylene Chain. *J. Am. Chem. Soc.* **1965**, *87*, 1415–1423.

(19) Paul, W.; Smith, G. D.; Yoon, D. Y.; Farago, B.; Rathgeber, S.; Zirkel, A.; Willner, L.; Richter, D. Chain Motion in an Unentangled Polyethylene Melt: A Critical Test of the Rouse Model by Molecular Dynamics Simulations and Neutron Spin Echo Spectroscopy. *Phys. Rev. Lett.* **1998**, *80*, 2346–2349.

(20) Smith, G.; Paul, W.; Monkenbusch, M.; Richter, D. A comparison of neutron scattering studies and computer simulations of polymer melts. *Chemical Physics* **2000**, *261*, 61 – 74.

(21) Krushev, S.; Paul, W.; Smith, G. D. The Role of Internal Rotational Barriers in Polymer Melt Chain Dynamics. *Macromolecules* **2002**, *35*, 4198–4203.

(22) Meyer, H.; Wittmer, J. P.; Kreer, T.; Beckrich, P.; Johner, A.; Farago, J.; Baschnagel, J. Static Rouse modes and related quantities: Corrections to chain ideality in polymer melts. *The European Physical Journal E* **2008**, *26*, 25–33.

(23) Kalathi, J. T.; Kumar, S. K.; Rubinstein, M.; Grest, G. S. Rouse Mode Analysis of Chain Relaxation in Homopolymer Melts. *Macromolecules* **2014**, *47*, 6925–6931.

(24) Mongcopa, K. I. S.; Tyagi, M.; Mailoa, J. P.; Samsonidze, G.; Kozinsky, B.; Mullin, S. A.; Gribble, D. A.; Watanabe, H.; Balsara, N. P. Relationship between Segmental Dynamics Measured by Quasi-Elastic Neutron Scattering and Conductivity in Polymer Electrolytes. *ACS Macro Letters* **2018**, *7*, 504–508.